Photocatalysis

Active Facets on Titanium(III)-Doped TiO₂: An Effective Strategy to Improve the Visible-Light Photocatalytic Activity**

Fan Zuo, Krassimir Bozhilov, Robert J. Dillon, Le Wang, Phillip Smith, Xiang Zhao, Christopher Bardeen, and Pingyun Feng*

The properties and applications of materials are significantly controlled by their physical characteristics, such as size, shape, and structural state. Many processes are governed by interface reactions by which the surface energy and reactivity depend on the spatial configuration, coordination, and structural state of surface atoms and molecules. For crystals, this dependence is directly related to the expression of specific crystallographic faces, which exhibit different surface structures and atomic configurations. These differences explain why some applications, such as molecular adsorption and desorption, gas sensing, drug molecule delivery and release, and heterogeneous catalysis are highly sensitive to the surface atomic structures. Recent progress in the engineering of crystal morphology has included the synthesis of polyhedral silver nanocrystals by the polyol method,[1] the epitaxially seeded growth of highly faceted Pt-Pd nanocrystals,[2] and the controlled overgrowth of Pd-Au core–shell structures enclosed by {111} facets.[3] Apart from these metallic nanocrystals, binary or ternary compounds with preferentially developed facets have also been reported.[4]

The facet effect is an important factor for heterogeneous photocatalysts, because surface atom arrangement and coordination intrinsically determine the adsorption of reactant molecules, surface transfer between photoexcited electrons and reactant molecules, and desorption of product molecules.[5] This phenomenon has been well studied in TiO₂ photocatalysts.[6] TiO₂ is one of the most extensively studied photocatalysts owing to its abundance, nontoxicity, and stability. However, for practical applications, pure TiO₂ is not a good candidate because it is only active under ultraviolet (UV) irradiation owing to the band gap of 3.2 eV for the anatase phase. Therefore, band-gap engineering is required to use TiO₂ as a water-splitting catalyst under visible-light irradiation. Reduced TiO₂ (TiO₂₋ₓ), containing Ti^{3+} or O vacancies, has been reported to show visible-light

absorption.[7] Various strategies have been applied to synthesize reduced TiO₂, such as heating under vacuum[8] or reducing gas,[9] laser irradiation,[10] and high-energy particle bombardment (electrons[11] or Ar⁺ ions[12]). A big challenge for the application of reduced TiO₂ is that the surface oxygen defects are highly unstable in air owing to the susceptibility of Ti^{3+} toward oxidation by O_2.[13] Recently, we reported a facile one-step combustion method to synthesize partially reduced TiO₂.[14] The presence of Ti^{3+} in the sample extends the photoresponse of TiO₂ from the UV to the visible light region, which leads to high visible-light photocatalytic activity for the generation of hydrogen gas from water. However, in the rapid and harsh combustion process, there is very limited control over the crystallization process, which results in the irregularly shaped products. Herein we report the development of a simple solution method to grow non-stoichiometric rutile TiO₂ crystals with desired facets. The incorporation of Ti^{3+}, which extends the light absorption from the UV into the visible range, along with the development of facets with high reactivity, results in a material exhibiting greatly enhanced photocatalytic H_2 production activity relative to the combustion product we reported before.

Powder X-ray diffraction analysis (Figure 1a) shows that the sample of as-produced TiO₂ (sample S1) has rutile structure. All of the diffraction peaks can be assigned to
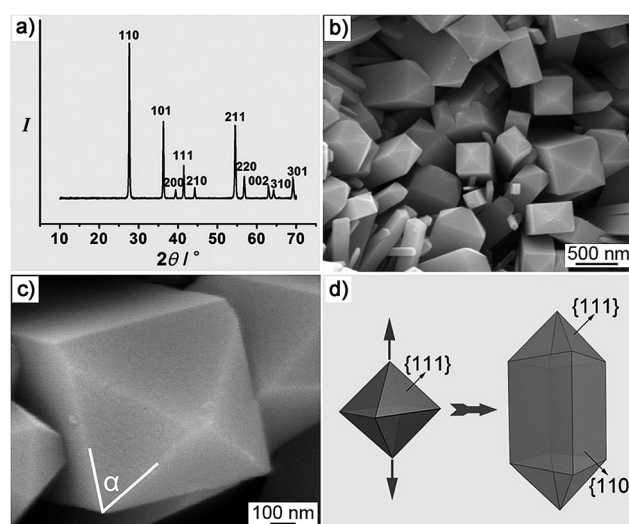
[*] F. Zuo, R. J. Dillon, L. Wang, P. Smith, X. Zhao, Prof. C. Bardeen, Prof. P. Feng
Department of Chemistry, University of California
Riverside, CA 92521 (USA)
E-mail: pingyun.feng@ucr.edu

Dr. K. Bozhilov
Central Facility for Advanced Microscopy and Microanalysis, University of California, Riverside (USA)

Supporting information for this article is available on the WWW under http://dx.doi.org/10.1002/anie.201202191.

Figure 1. a) XRD pattern of an as-prepared sample obtained by hydrothermal treatment of Ti powder and HCl under 220°C for 12 h. b) Typical SEM image of the rutile crystal: a tetragonal prism with a pyramid-like top. c) High-magnification SEM image showing the top feature of the crystal. d) The faceting process of the rutile TiO₂.

© 2012 Wiley-VCH Verlag GmbH & Co. KGaA, Weinheim
WILEY ONLINE LIBRARY **6223**

tetragonal rutile structure with cell parameters $a = 4.584$ Å and $c = 2.953$ Å, space group $P4_2/mnm$ (JCPDS No. 89-4920). No anatase diffraction peaks are observed. Figure 1b shows a typical scanning electron microscopy (SEM) image of the as-synthesized sample. This hydrothermal method produces tetragonal crystals with a prismatic habit that are obviously different from the irregular particles we previously prepared (sample S2; Figure S1). Based on first-principles calculations, the crystal face with the lowest surface free energy for rutile is {110},[15] a form which is preferentially developed in the crystals from this sample. A high-magnification SEM image (Figure 1c) reveals that the rutile crystals are a combination of prismatic and bipyramidal forms. The angle α of (53.6°) measured between the edges of the prismatic and pyramidal facets (Figure 1c) matches closely the theoretical value between the $\langle 110 \rangle$ and $\langle 011 \rangle$ directions in a tetragonal lattice with $a = 4.584$ Å and $c = 2.953$ Å. From the above investigation, we can propose that the rutile crystals in sample S1 are a combination of a {110} tetragonal prism and a {111} tetragonal bipyramid, with preferentially developed {110} prismatic faces, which gives the crystals an elongated habit along the c axis (Figure 1d). This interpretation is unambiguously supported by transmission electron microscopy (TEM). Figure 2a shows a TEM image of a representative

Figure 2. a) Typical TEM image of a rutile TiO_2 single crystal. The overlaid inset is the oriented [110] SAED pattern from this crystal. b) High-resolution TEM image taken from the circled area in (a). c) EPR spectra measured at 100 K. d) UV/Vis diffuse reflectance spectra for commercial P25 (•••••) and S1 (——).

rutile single crystal, and the corresponding selected area electron diffraction (SAED) pattern, which is overlaid on top of the crystal image. The spot SAED pattern clearly demonstrates the single-crystal nature of the individual grains of this sample. The SAED pattern was taken with the electron beam normal to one of the prismatic faces of the

crystal. Inspection of the indexed [110] zone axis pattern reveals that the prismatic crystal faces are parallel to {110}, the bipyramid faces are parallel to {111}, and the elongation of the crystal is parallel to $\langle 001 \rangle$. This is confirmed by the high-resolution TEM (HRTEM) image taken from the marked area in the low-magnification TEM image (Figure 2b), which reveals the crystal lattice and the orientation of the lattice planes with respect to the crystal faces. The lattice fringes of 3.22 Å and 2.95 Å correspond to the {110} and {001} lattice spacing, respectively, corroborating the SAED measurements.

Electron paramagnetic spectra (EPR) were recorded at 100 K to determine the presence of Ti^{3+}. A strong EPR signal is observed at $g = 1.97$ (Figure 2c), which could be assigned to Ti^{3+},[16] thus confirming the existence of the Ti^{3+} in the synthesized sample (Figure 2c). The presence of Ti^{3+} may result from reduction of Ti^{4+} by H_2, which is produced by the reaction between Ti powder and HCl (details are presented in the Supporting Information). It is worth noting that the EPR spectra also excludes the presence of Ti^{3+} on the surface of the sample, as the surface Ti^{3+} is prone to adsorb atmospheric O_2, which would be reduced to O_2^- and will show an EPR signal at $g \approx 2.02$,[17] which is absent in our spectrum. The XPS study further confirmed that no Ti^{3+} exists on the surface (Supporting Information, Figure S2). Having all of the Ti^{3+} located in the bulk is crucial for the stability of our non-stoichiometric TiO_2 sample, as the surface oxygen defects are not usually stable enough to survive in air and are even susceptible to oxidation by dissolved oxygen in water.[13,18] The concentration of Ti^{3+} was determined by numerical double integration of EPR spectra and comparison with a frozen aqueous solution of Cu^{2+}. The concentration of Ti^{3+} was estimated to be 4.95 $\mu mol\,g^{-1}$ with an absolute accuracy of about $\pm 20\%$.[19]

Figure 2d shows the UV/Vis absorption spectra for the sample and the commercial Dequssa P25 (a mixture of anatase and rutile TiO_2). Compared to the stoichiometric TiO_2, the partially reduced sample shows a red-shift in the spectrum, which suggests a decrease in the band gap. Our calculation has demonstrated that the Ti^{3+} inside the bulk TiO_2 could induce a vacancy band of electronic states just below the conduction band, which is responsible for the band gap narrowing.[14] The assumption of a miniband also explains why the absorbance in the visible range for the as-prepared sample is stronger than that for Ti^{3+} free P25.

The photocatalytic activity of the sample for hydrogen production from water was tested. After loading a sample (0.100 g) with 1% Pt (0.001 g), the photocatalyst S1 was placed into an aqueous methanol solution (120 mL, 25%) in a closed-gas circulation system. A Xe lamp (300 W) with a 400 nm cut-on filter was used to cut off the UV light and allow only visible light (>400 nm) to pass through. Figure 3 shows the time course of H_2 evolution for as-prepared sample S1. Under the above reaction conditions, the sample could steadily produce hydrogen gas at about 18.1 $\mu mol\,h^{-1}/0.100$ g. After illumination for 100 h, 1843 $\mu mol\ H_2$ was evolved in total, which accounts for a turnover number of 1.47. This result confirms the H_2 production is a photocatalytic process. Note that no noticeable decrease in H_2 production rate was observed within the 100 h photocatalytic period (Supporting
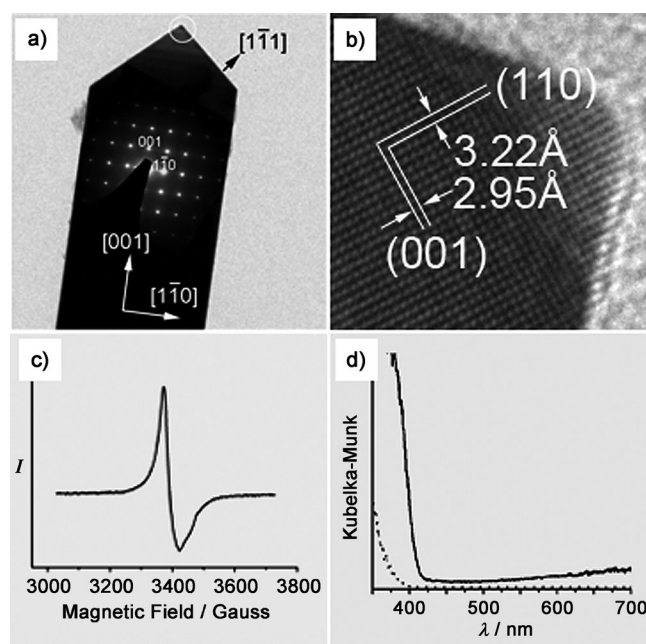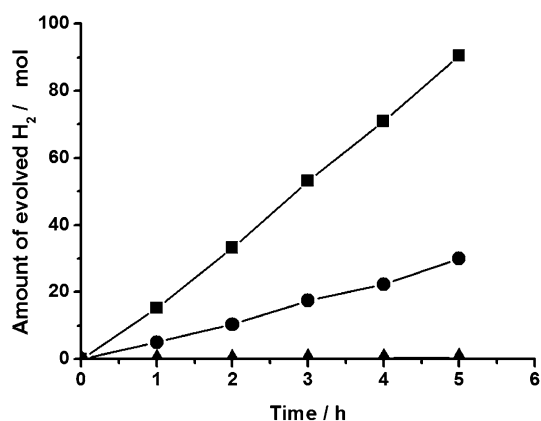
Figure 3. Time course of evolved H$_2$ under visible light (> 400 nm) illumination. (■) Sample S1, reduced TiO$_2$, tetragonal prism; (●) Sample S2, reduced TiO$_2$, irregular nanoparticles; (▲) Sample S3, stoichiometric TiO$_2$, tetragonal prism.

Information, Figure S3), thus demonstrating the high stability of the photocatalyst. We measured the external quantum efficiency (EQE) with a 420 nm band pass filter, which gave an EQE value of 2.28%.

The effect of the active facets is investigated by comparing sample S1 with our previously reported reduced TiO$_2$ irregular nanoparticles S2. Under the same photoreaction conditions, S1 exhibits 200% improvement (18.1 µmol h^{-1}/0.100 g versus 6.0 µmol h^{-1}/0.100 g), which strongly demonstrates the enhancement of the photocatalytic activity owing to the active facets. We have measured the surface area of these samples and find that S1 has a much lower surface area than S2 (5.5 m^2 g^{-1} versus 11.7 m^2 g^{-1}), even though its activity is much higher. This decrease in surface area would be expected to lower the catalytic activity of S1, which is contrary to what is observed. Thus the increased activity of S1 must result from some other feature of its morphology. It has been reported that {111} and {110} facets are prone to collect holes and electrons, respectively,[20] which greatly improves the separation of holes and electrons. SEM imaging of sample S1 after the photocatalytic reaction (Supporting Information, Figure S5) revealed that no deformation or size and shape changes have taken place during the photocatalytic reaction. Of greater importance is the observation that the Pt nanoparticles accumulated exclusively on the {110} facets, without any Pt nanoparticles found on the {111} facets. This observation confirms that the photogenerated electrons selectively gathered on the {110} facets, where the Pt^{IV} was reduced to Pt nanoparticles. To further examine how the shape of the particle influences the electron–hole dynamics, we compared the fluorescence decays from samples S1 and S2. Both samples show the highly nonexponential decay of fluorescence centered around 480 nm that has previously been attributed to surface trap states.[21] The distribution of surface traps, with different lifetimes, is what leads to the highly nonexponential decays. However, in S1, where the {111} and {110} facets are well-defined, the fluorescence lifetime is significantly longer than in the irregularly shaped S2 sample. Although we cannot extract a single decay time, the 1/e decay

time is almost twice as long for the S1 sample at room temperature (Supporting Information, Figure S6). This difference becomes more pronounced at lower temperatures (Supporting Information, Figure S7). At 84 K, the S1 1/e decay time is almost four times longer, and it is clear that the short-time decay in S2 is much reduced in S1. If we attribute the fluorescence decay to recombination of the surface trapped electron or hole with its counterpart, then it appears that rapid recombination events play a smaller role in S1. If electrons and holes are trapped at crystallographically different crystal facets, such as the {111} and {110} in the S1 sample, then this effective separation of the electron and hole would suppress rapid recombination events, as observed experimentally. Slower electron–hole recombination would provide the trapped charges with more opportunities to initiate surface reactions, thus presumably enhancing the photocatalytic activity as observed for these particles as well. We also ran a control experiment on a stoichiometric rutile TiO$_2$ sample with active facets (sample S3) formed by heating S1 in air under 210°C for 8 h. After oxidation, S3 retains the original prismatic shape of the S1 sample (Supporting Information, Figure S8) but almost completely loses its photocatalytic activity (< 0.1 µmol h^{-1}/0.100 g). EPR measurements show no presence of Ti^{3+} in the S3, and the UV/Vis spectra reveal that the absorbance of visible light (wavelength greater than 400 nm) is nearly extinguished (Supporting Information, Figure S9). This control experiment demonstrates that it is the Ti^{3+} that effectively extends the photoresponse of TiO$_2$ from UV to visible light region, resulting in the visible-light activity of the as-synthesized S1.

In conclusion, we have synthesized a partially reduced non-stoichiometric rutile TiO$_2$ with active facets by a facile solution method. This highly stable photocatalytic material has a greatly improved efficiency to reduce water when compared to irregularly shaped nanoparticles. The new synthetic approach presented herein provides a way to control the final crystal morphology of the target product. We expect to utilize this new strategy to explore how the interplay of chemical composition and nanoscale morphology affects the photocatalytic activity of TiO$_2$, with the ultimate goal of finding new and highly efficient photocatalysts.

Experimental Section

All chemicals, including titanium powder (Aldrich, 99%) and hydrochloric acid (Fisher scientific, 37.1%), were used as received without any further purification. In a typical synthetic procedure, titanium powder (0.300 g) and hydrochloric acid (10 mL, 2 M) were mixed in a 50 mL pyrex beaker and magnetically stirred for 15 min. This mixture was then transferred to the Teflon-lined stainless-steel autoclave (23 mL capacity) and hydrothermally treated for 12 h under 220°C. The sample was then collected and washed by distilled water and ethanol three times.

[1] A. Tao, P. Sinsermsuksakul, P. D. Yang, *Angew. Chem.* **2006**, *118*, 4713 – 4717; *Angew. Chem. Int. Ed.* **2006**, *45*, 4597 – 4601.

[2] S. E. Habas, H. Lee, V. Radmilovic, G. A. Somorjai, P. Yang, *Nat. Mater.* **2007**, *6*, 692 – 697.

[3] B. Lim, H. Kobayashi, T. Yu, J. G. Wang, M. J. Kim, Z. Y. Li, M. Rycenga, Y. N. Xia, *J. Am. Chem. Soc.* **2010**, *132*, 2506 – 2507.

[4] a) B. Sadtler, D. O. Demchenko, H. Zheng, S. M. Hughes, M. G. Merkle, U. Dahmen, L. W. Wang, A. P. Alivisatos, *J. Am. Chem. Soc.* **2009**, *131*, 5285 – 5293; b) Y. Bi, S. Ouyang, N. Umezawa, J. Cao, J. Ye, *J. Am. Chem. Soc.* **2011**, *133*, 6490 – 6492; c) G. C. Xi, J. H. Ye, *Chem. Commun.* **2010**, *46*, 1893 – 1895.

[5] G. Liu, J. C. Yu, G. Q. Lu, H. M. Cheng, *Chem. Commun.* **2011**, *47*, 6763 – 6783.

[6] a) H. G. Yang, C. H. Sun, S. Z. Qiao, J. Zou, G. Liu, S. C. Smith, H. M. Cheng, G. Q. Lu, *Nature* **2008**, *453*, 638 – 634; b) G. Liu, H. G. Yang, X. W. Wang, L. N. Cheng, J. Pan, G. Q. Lu, H. M. Cheng, *J. Am. Chem. Soc.* **2009**, *131*, 12868 – 12869; c) G. Liu, C. H. Sun, H. G. Yang, S. C. Smith, L. Z. Wang, G. Q. Lu, H. M. Cheng, *Chem. Commun.* **2010**, *46*, 755 – 757; d) J. Pan, G. Liu, G. M. Lu, H. M. Cheng, *Angew. Chem.* **2011**, *123*, 2181 – 2185; *Angew. Chem. Int. Ed.* **2011**, *50*, 2133 – 2137; e) M. D'Arienzo, J. Carbajo, A. Bahamonde, M. Crippa, S. Polizzi, R. Scotti, L. Wahba, F. Morazzoni, *J. Am. Chem. Soc.* **2011**, *133*, 17652 – 17661; f) E. Hosono, S. Fujihara, K. Kakiuchi, H. Imai, *J. Am. Chem. Soc.* **2004**, *126*, 7790 – 7791.

[7] a) R. D. Iyengar, M. Codell, *Adv. Colloid Interface Sci.* **1972**, *3*, 365 – 388; b) D. C. Cronemeyer, *Phys. Rev.* **1959**, *113*, 1222 – 1226.

[8] E. Serwicka, *Colloid Surface* **1985**, *13*, 287 – 293.

[9] G. M. Wang, H. Y. Wang, Y. C. Ling, Y. C. Tang, X. Y. Yang, R. C. Fitzmorris, C. C. Wang, J. Z. Zhang, Y. Li, *Nano Lett.* **2011**, *11*, 3026 – 3033.

[10] N. Ohtsu, K. Kodama, K. Kitagawa, K. Wagatsuma, *Appl. Surf. Sci.* **2010**, *256*, 4522 – 4526.

[11] G. A. Kimmel, N. G. Petrik, *Phys. Rev. Lett.* **2008**, *100*, 196102.

[12] S. Hashimoto, A. Tanaka, *Surf. Interface Anal.* **2002**, *34*, 262 – 265.

[13] A. Teleki, S. E. Pratsinis, *Phys. Chem. Chem. Phys.* **2009**, *11*, 3742 – 3747.

[14] F. Zuo, L. Wang, T. Wu, Z. Y. Zhang, D. Borchardt, P. Y. Feng, *J. Am. Chem. Soc.* **2010**, *132*, 11856 – 11857.

[15] A. S. Barnard, L. A. Curtiss, *Nano Lett.* **2005**, *5*, 1261 – 1266.

[16] J. C. Conesa, J. Soria, *J. Phys. Chem.-Us* **1982**, *86*, 1392 – 1395.

[17] M. Anpo, M. Che, B. Fubini, E. Garrone, E. Giamello, M. C. Paganini, *Top. Catal.* **1999**, *8*, 189 – 198.

[18] K. Komaguchi, T. Maruoka, H. Nakano, I. Imae, Y. Ooyama, Y. Harima, *J. Phys. Chem. C* **2010**, *114*, 1240 – 1245.

[19] R. F. Howe, M. Gratzel, *J. Phys. Chem-Us* **1985**, *89*, 4495 – 4499.

[20] a) T. Ohno, K. Sarukawa, M. Matsumura, *New J. Chem.* **2002**, *26*, 1167 – 1170; b) E. Bae, N. Murakami, T. Ohno, *J. Mol. Catal. A* **2009**, *300*, 72 – 79.

[21] K. Fujihara, S. Izumi, T. Ohno, M. Matsumura, *J. Photochem. Photobiol. A* **2000**, *132*, 99 – 104.